5 Process-based modelling of long-term channel–shoal pattern formation [1]

Abstract

The formation of channel and shoal patterns in a schematic estuary is investigated using a 2-D depth-averaged numerical model based on a description of elementary flow and sediment transport processes. The schematisations apply to elongated inland estuaries, sandy, well-mixed and tide-dominated. The model results show how, due to non-linear interactions, a simple and regular pattern of initially grown perturbations merges to complex larger scale channel–shoal patterns. The emerging patterns are validated with field observations. The overall pattern agrees qualitatively with patterns observed in the Western Scheldt estuary, The Netherlands, and in the Patuxent River estuary, Virginia. Quantitative comparison of the number of channels and meander length scales with observations and with an analytical model gives reasonable accordance. Complementary to other research approaches, this model provides a tool to study the morphodynamic behaviour of channels and shoals in estuaries.

5.1 Introduction

Channels and shoals are important features in estuaries and tidal inlets. The channels provide access to harbours further inland, and the intertidal areas are important feeding and breeding grounds for a variety of species and are thus of great ecological importance.

Comparable phenomenological descriptions of channel–shoal systems, based on observations, are published by Van Veen (1950) for the Dutch tidal waters, Ahnert (1960) for estuaries around Chesapeake Bay, USA and Robinson (1960) for estuaries in Great Britain. These authors categorised the channels as ebb- and flood-dominated. An important characteristic of these ebb- and flood-channels is that they seem to evade one another. Van Veen explained this from the

1. This chapter has been published as: A. Hibma, H.J. de Vriend and M.J.F. Stive, 2003. Numerical modelling of shoal pattern formation in well-mixed elongated estuaries. *Estuarine, Coastal and Shelf Science Vol. 57, 5-6, p.981-991*

difference in meander action between ebb and flood, and from the opposite directions of the sand streams in those channels, which leads to the formation of a bar or threshold where they meet. His analyses are based on observations.

At present, despite the availability of modern computing techniques, estuaries are still difficult to model, because the behaviour of channel–shoal systems is complex and involves a wide range of space and time scales (De Vriend, 1996). The formation of channels and shoals in estuaries cannot always be attributed to spatial and temporal variations of external forcing factors and must therefore be a manifestation of free behaviour inherent to the system. The capability to predict channel and shoal behaviour is of great practical interest, for economical as well as environmental aspects of estuarine management. Therefore, a better insight into the physical mechanisms behind this aspect of estuarine morphodynamics is worth pursuing.

The tidal motion is used as a driving mechanism in several studies to determine the one-dimensional morphodynamic equilibrium profiles of estuaries (Boon and Byrne, 1981; Friedrichs and Aubrey, 1996; Schuttelaars and De Swart, 1996; Lanzoni and Seminara, 2002). Studies of the 2-dimensional long-term interaction between channels and shoals in estuaries are scarce and the understanding of shoal genesis is still limited (Dalrymple and Rhodes, 1995). Beside field observations and laboratory experiments (Bolla Pittaluga et al., 2001) various model approaches can be used to investigate the mechanisms behind channel–shoal interactions (De Vriend, 1996; De Vriend and Ribberink, 1996; Di Silvio and Padovan, 1998) uses a 2-dimensional model in which the morphological evolution is driven by the action of waves and tidal currents via the definition of an appropriate equilibrium concentration.

The approach of Seminara and Tubino (1998) and Schuttelaars and De Swart (1999) is based on stability analysis and focuses on the initial formation of the channel–shoal pattern. These authors determine the growth rate of small-amplitude undulations (modes) as a function of the wave number vector. Their analyses demonstrate that growing free modes can occur. Such analyses are linear and therefore restricted to initial exponential growth, or weakly non-linear and therefore restricted to patterns close to the linearly most unstable mode. Moreover, they are practically restricted to idealised situations.

The physical processes included in these idealised models and held responsible for the formation of channels and shoals are also captured in the more complex process-based numerical modelling system Delft3D (Wang et al., 1992, 1995b). This system is based on coupled descriptions of small-scale hydrodynamic and sediment transport processes, and steps forward through time by updating the bed topography using sediment mass balance. A model based on this system should therefore be able to reproduce morphological features such as channels and shoals. Once the model has been validated, it can be used to gain insight into the underlying mechanisms. Moreover, computations with this validated model can be carried further into the domain of strongly non-linear interaction and more complex geometries.

The overall objective of the study described herein is to improve the knowledge of the mechanisms responsible for the formation of channels and shoals in sandy estuaries. The main thrust of the present paper is to assess to what extent a 2-D depth-averaged process-based model reproduces this phenomenon. Like Seminara and Tubino (1998) and Schuttelaars and De Swart (1999), an idealised sandy estuary of constant width is considered, in order to come to grips with the physical processes. The initial model results are compared to those of the analytical approach. The emerging channel–shoal pattern is validated with field data.

5.2 Numerical model description

The Delft3D modelling system is designed to simulate wave propagation, currents, sediment transport, morphological developments and water quality in coastal, river and estuarine areas (Roelvink and van Banning, 1994; Verbeek et al., 1999). Delft3D is a finite-difference system in which the processes are simulated on a curvilinear grid allowing for an efficient and accurate representation of complex domains. The computational grid is staggered, with the water level, the water depth and the velocity components all defined at different locations within a grid cell (Stelling, 1984). The principal constituents of an estuarine morphodynamic model are the flow, sediment transport and bottom change modules. These will be described below.

5.2.1 Flow

The flow module computes unsteady flow resulting from tidal and meteorological forcings. It is based on the shallow water equations. In this study, the 2DH (2–D depth-averaged) mode is applied and density differences are neglected, thereby constraining the model to well-mixed situations. The depth averaged equations for conservation of momentum in x- and y-direction are given by:

$$\frac{\partial u}{\partial t} + u\frac{\partial u}{\partial x} + v\frac{\partial u}{\partial y} + g\frac{\partial \eta}{\partial x} - fv + \frac{gu|U|}{C^2(d+\eta)} - \frac{F_x}{\rho_w(d+\eta)} - \nu\left(\frac{\partial^2 u}{\partial x^2} + \frac{\partial^2 u}{\partial y^2}\right) = 0 \qquad (5.1)$$

and

$$\frac{\partial v}{\partial t} + u\frac{\partial v}{\partial x} + v\frac{\partial v}{\partial y} + g\frac{\partial \eta}{\partial y} + fu + \frac{gv|U|}{C^2(d+\eta)} - \frac{F_y}{\rho_w(d+\eta)} - \nu\left(\frac{\partial^2 v}{\partial x^2} + \frac{\partial^2 v}{\partial y^2}\right) = 0 \qquad (5.2)$$

The depth averaged continuity equation is given by:

$$\frac{\partial \eta}{\partial t} + \frac{\partial u(d+\eta)}{\partial x} + \frac{\partial v(d+\eta)}{\partial y} = 0 \qquad (5.3)$$

in which:

C : Chézy coefficient ($m^{1/2}/s$)
d : water depth w.r.t. MSL (m)
g : gravitational acceleration (m^2/s)
f : Coriolis parameter (s^{-1})
$F_{x,y}$: x- and y-component of external forces due to wind and waves (N/m^2)
u, v : depth-averaged velocity components (m/s)
U : magnitude of total velocity, $U = (u^2 + v^2)^{1/2}$ (m/s)
ρ_w : mass density of water (kg/m^3)
ν : diffusion coefficient (eddy viscosity) (m^2/s)
η : water level (m)

Drying and flooding

In tidal areas the shallow parts become dry during low tide. In the FLOW-module, flooding and drying is represented by removing grid cells that become dry when the tide falls, and reactivating cells that become wet when the tide rises. If the total water depth in a velocity point is below a certain threshold (0.1 m in this study), this point is set dry, which means that the velocity is set equal to zero. The computational cell is closed at the side normal to the velocity. If the water level rises and the total water depth is greater than twice the threshold, the velocity point is reactivated. When all four velocity points of a computational cell surrounding a water level point are dry, this cell is excluded from the computation.

5.2.2 Sediment transport

The sediment transport is determined, with access to a variety of semi-empirical formulae and a depth integrated advection-diffusion solver for suspended sediment. The transport computations are based on the time-dependent current fields.

Two different sediment transport options for non-cohesive sediment were tested in this study. First, a total-load transport formula, where the total sediment transport is the sum of bed load and equilibrium suspended load transport. In this study the transport relation of Engelund and Hansen (1967) is used:

$$S = S_b + S_{se} = \frac{0.05\alpha U^5}{g^{0.5} C^3 \delta^2 d_{50}} \tag{5.4}$$

where:

α : calibration coefficient
δ : the relative density $(\rho_s - \rho_w)/\rho_w$
d_{50} : characteristic grain size (m)

The other option is to derive the bed load transport and the local equilibrium concentration c_{se} from algebraic sediment transport formulae and determine the actual suspended sediment concentrations and transport rates from an advection-diffusion equation for the suspended sediment concentration.

For simulations where this more advanced option is applied, the transport formula of Van Rijn (1984) is used to calculate bed load transport (S_b) and the equilibrium suspended sediment transport rate (S_{se}):

$$S_b = \begin{cases} 0.053(\delta g d_{50})^{0.5} {D_*}^{-0.3} T^{2.1} & \text{for} \quad T < 3.0 \\ 0.1(\delta g d_{50})^{0.5} {D_*}^{-0.3} T^{1.5} & \text{for} \quad T \geq 2.1 \end{cases} \tag{5.5}$$

$$S_{se} = f_{cs} U h C_a \tag{5.6}$$

with:

$$C_a = \frac{0.015 \alpha_1 d_{50} T^{1.5}}{\zeta_c {D_*}^{0.3}} \tag{5.7}$$

in which:

C_a	: reference concentration, at the effective bed roughness height above the bed (kg/m^3)
ζ_c	: roughness height (m)
α_1	: coefficient, $O(1)$
D_*	: grain size parameter $d_{50}(\delta g/\nu^2)^{1/3}$
f_{cs}	: shape factor
h	: water depth (m)
T	: dimensionless bed shear parameter, written as $T = \frac{\mu_c \tau_{bc} - \tau_{b\tau}}{\tau_{bcr}}$
τ_{bcr}	: critical shear stress according to Shields (N/m^2)
$\mu_c \tau_{bc}$	: shear stress (N/m^2)

The sum of Eqs. 5.5 and 5.6 gives a total-load transport formula, analogous to Engelund and Hansen. For the advanced option with an advection-diffusion equation, the depth averaged equilibrium concentration is subsequently derived from the equilibrium suspended transport rate by:

$$c_{se} = \frac{S_{se}}{\alpha_s U h} \tag{5.8}$$

in which α_s is a dimensionless shape factor.

Then the advection-diffusion equation for suspended sediment is solved, which reads:

$$\frac{\partial hc_s}{\partial t} + \alpha_u \left(u\frac{\partial hc_s}{\partial x} + v\frac{\partial hc_s}{\partial y} \right) + \frac{\partial}{\partial x}\left(\epsilon_x h \frac{\partial c_s}{\partial x} \right) + \frac{\partial}{\partial y}\left(\epsilon_y h \frac{\partial c_s}{\partial y} \right) = \gamma w_s (c_{se} - c_s) \tag{5.9}$$

where:

ϵ_x, ϵ_y : dispersion coefficient (m^2/s)
c_s : concentration of suspended sediment (m^3/m^3)
c_{se} : equilibrium concentration of suspended sediment (m^3/m^3)
w_s : fall velocity of suspended sediment (m/s)

The dimensionless coefficients α_u and γ include the 3D effects and can be calculated according to Gallappatti and Vreugdenhill (1985). γ is dependent on w_s, the depth averaged velocity and the bed shear stress velocity. In this study, α_u is taken 1.0 for simplicity.

In this suspended transport model, boundary conditions have to be prescribed at all open boundaries. The mouth of the estuary is an open boundary. Here, the outflow concentration is set equal to the concentration just landward of the boundary and the inflow concentration corresponds to local equilibrium conditions.

Finally, the total load or the bed load as well as the suspended load sediment transport is multiplied by a factor of $O(1)$ that takes into account the downhill gravitational component of the transport.

5.2.3 Bed evolution

The bed level changes due to gradients in the sediment transport fields. The determination of the bed evolution is based on the conservation of sediment mass:

$$\frac{\partial hc_s}{\partial t} + (1 - \epsilon_{por})\frac{\partial z_a}{\partial t} + \left(\frac{\partial S_x}{\partial x} + \frac{\partial S_y}{\partial y} \right) = 0 \tag{5.10}$$

in which:

z_a : bed level (m)
S_x, S_y : sediment transport in x- and y-direction ($m^3/m/s$)
ϵ_{por} : bed porosity

The interest is in longer-term bed changes and the bed level update determined from Eq. 5.10 is integrated over a tidal cycle. Then the term $\frac{\partial hc_s}{\partial t}$ is small and therefore neglected.

5.2.4 Process–compiling

The model input and output of the above described process modules are linked in a steering module. The morphological process is modelled as a hierarchical tree structure of components.

The user defines the sequence of module calls and the time progress. The steering module for the simulations in this study consist of a loop in which a flow-module is called for one tidal period, followed by a transport computation for each phase of this tidal period. Eq. 5.10 is then solved using an explicit scheme of the Lax-Wendroff type, updating the bathymetry from the divergence of the tidally averaged sediment transport field. In this study, the time-step during which this bottom update can be increased linearly is determined automatically, on the basis of the Courant number for bed level perturbations. The process-loop is repeated with every updated bathymetry, till the prescribed stop time is reached.

5.3 Model schematisation

The idealised estuary on which this paper focuses is 80 km long and has a constant width of 2.5 km (see Fig. 5.1). The underlying grid has a mesh size of 250 m x 125 m in longitudinal and transverse direction, respectively. The initial bottom level is 15 m below MSL at the seaward end, linearly decreasing to zero at the landward boundary and constant over the width. The lateral and landward boundaries are fixed and impermeable. The bed material consists of uniform sand with $d_{50} = 240\mu m$. The initial bed-level is given random small-amplitude perturbations, by adding a random value to the depth value of each gridcell. These initial disturbances maximally amount to plus or minus 5% of the water depth. At the entrance of the estuary a periodic water level boundary is imposed to simulate the M_2 tidal component with an amplitude of 1.75 m. For the bottom roughness, a constant Manning coefficient of 0.026 $m^{1/3}/s$ is used. Waves and Coriolis-effect are neglected. This model thereby simulates a tide-dominated basin that falls in the meso-tidal category of Hayes (1975).

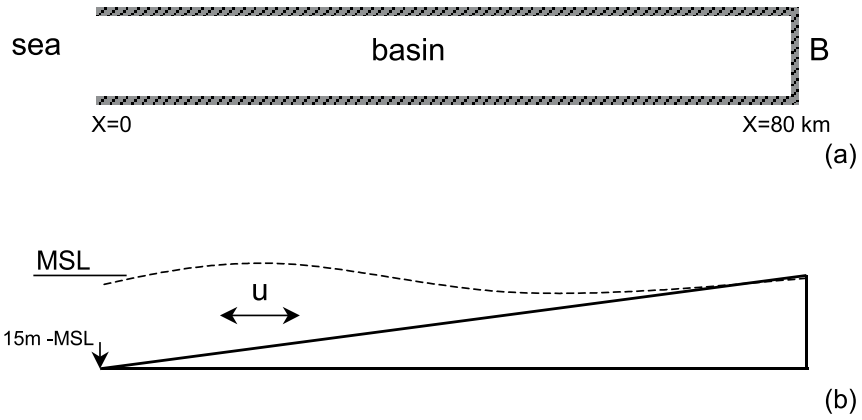

Figure 5.1: Upper panel: top view of estuary. Lower panel: side view of estuary.

5.4 Model results

A model simulation for 120 years has been made. The first bathymetric structure becomes visible after 10 years at the landward part of the estuary. Subsequently, this initial pattern of 3–D undulations arises upstream and downstream. The structure gradually changes, which eventually leads to the formation of channels and shoals as shown in Fig. 5.2.

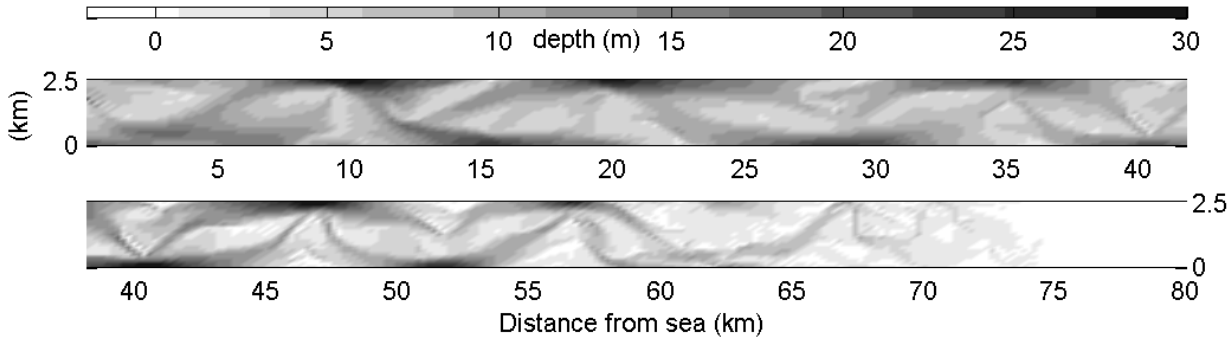

Figure 5.2: Bathymetry after 120 years. Upper panel: seaward end. Lower panel: landward end.

The channel and shoal pattern develops a meandering ebb channel and flood dominated overshoots, separated by shoals (the trajectories of the residual flow is shown in Fig. 5.4). The channels are alternating aligned with the lateral boundaries of the estuary and form a repeating pattern in longitudinal direction. The wavelength decreases from 15 km at the entrance to 10 km in the landward part of the estuary. After a simulated period of 120 years, the channels have reached depths of 25 to 35 m, but contain bars/thresholds where the water depth is only 10 to 15 m. The shoals reach heights of around MSL and can fall dry during low water. In some gridcells the bed reaches unrealistic heights above the high water level. This is a model artifact, due to very large bed-level updates just before these gridcells fall dry during the tidal cycle. By decreasing the time-step for the bottom update this artifact could be avoided. However, the overall pattern is not influenced by decreasing the time-step, but the computation time increases, so the longer time-step is used to enable the long-term simulations.

A more detailed view on the development of the channels and shoals is presented in Fig. 5.3, showing the middle part of the estuary. In the shallow landward side the first undulations become visible between 10 and 15 years (second and third panels). The wavelength of these undulations is 3 km in longitudinal and 2.5 km in transverse direction. After some time, this pattern gradually changes into a formation in which the deeper parts connect and form meandering channels, accompanied by some migration (fourth to sixth panels). These connecting channels merge to broader channels, revealing a larger wavelength (seventh panel). After 50 years the pattern has almost evolved to its final stage (eighth panel). At the end of the simulation, the wavelength has increased to 12 km and there is no consistent migration (ninth panel).

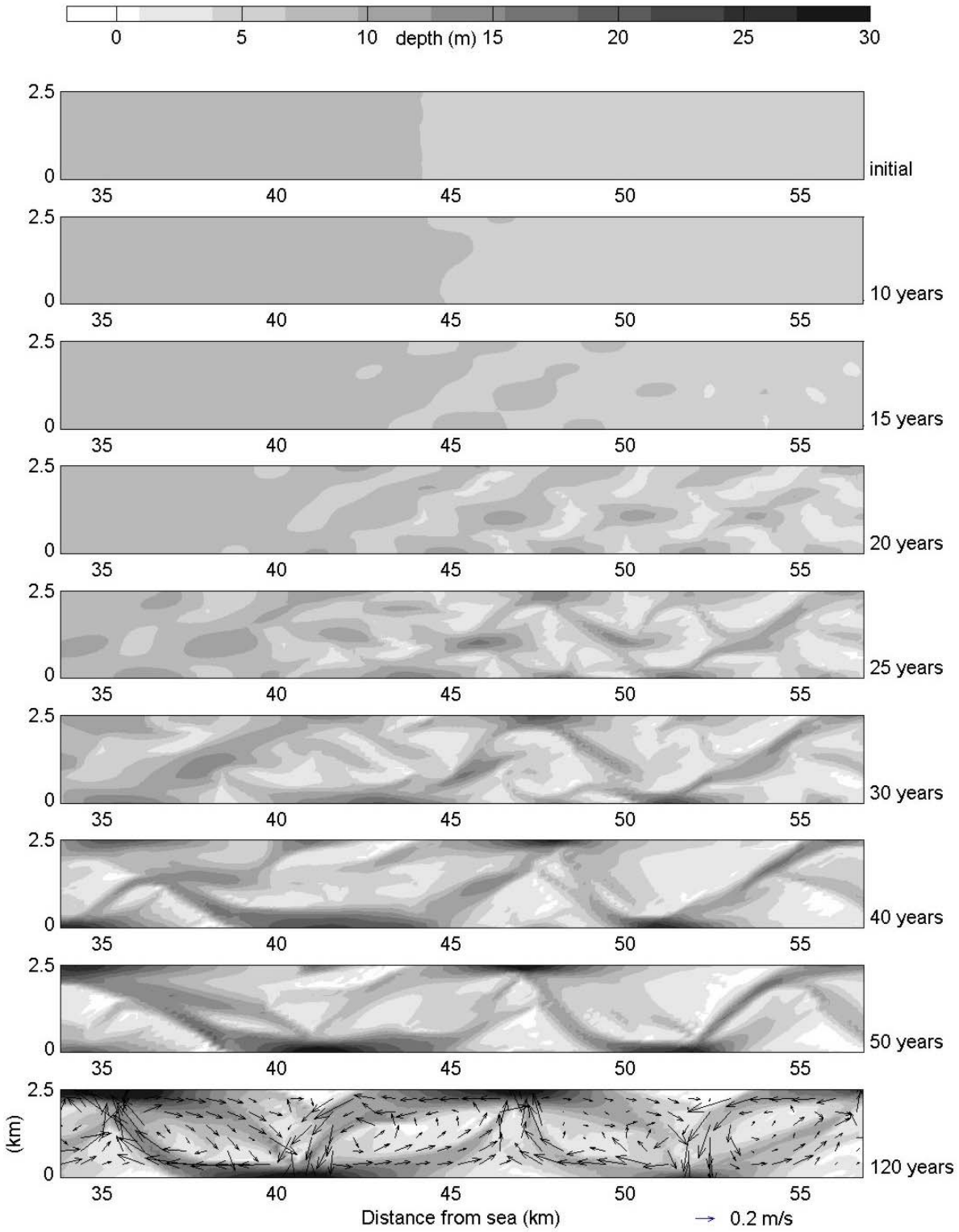

Figure 5.3: Formation of channels and shoals halfway up the estuary. The arrows in the last panel indicate the velocity magnitude and direction of the tidally-averaged flow pattern from the model simulation.

The first scour holes and deposition areas form more slowly in the deeper seaward part. They form an alternating pattern, with a wavelength in the longitudinal direction of 7 to 10 km (upper panel Fig. 5.2, i.e. considerably larger than in the shallow parts of the estuary. The evolution of the pattern is similar to that in the shallow part, showing migration and an increase of wavelengths. This pattern evolution slows during the simulation and the global pattern is more or less fixed after 100 years. Locally, at the crossings of the channels, the bathymetry remains highly dynamic, as the channel ends move to and fro.

The above simulation uses the total load transport formula of Engelund and Hansen (1967). When the Van Rijn formulations (1984) for total load transport are used, the initial results are similar, though the time scales differ. Using Van Rijn's formulations, the growth of the erosional and depositional areas is initially slower in the landward area, while it is slightly faster at the mouth of the model estuary. This is probably due to the smaller exponent in the transport relationship, and by the inclusion of a threshold of motion. The development of the channel–shoal pattern is largely analogous, but local differences exist.

Van Rijn's relationships are also used for the equilibrium concentration and the bed-load transport rate when the advection-diffusion solver for suspended sediment is applied. Using this option, the dispersion coefficient is set at 10 m^2/s (Fischer, 1979). The adaptation length of the sediment concentration, defined by the water depth times the current velocity divided by the fall velocity of the sediment is typically 500 m. Due to this modulation of suspended load transport, the emerging initial pattern is somewhat smoother in this case. The location and wavelength of the initial undulations remain similar to the previous cases. The time needed for the initial pattern to become visible is longer than in the total-load transport case, probably due to the smoothing effect of suspended transport, which forms the main transport mode. The bed load transport accounts for less than 10% of the suspended load transport. During the transition to the channel–shoal pattern, the shoals attain greater heights probably due to lag-effects. In the shallow landward part of the estuary, the pattern deviates from those seen before. Three to four meandering channels are formed in parallel, separated by shoals. This pattern remains stable.

5.5 Validation with field data

The model is validated against field observations by Van Veen (1950) and Ahnert (1960). Ahnert studied the estuaries around the Chesapeake Bay, Maryland, USA. The main interest of Van Veen is the Western Scheldt estuary in The Netherlands. This 160 km long funnel-shaped estuary, with an entrance width of 6 km, exhibits a well-developed system of channels and shoals. In his characterisation of channel patterns in estuaries, Van Veen categorised channels as ebb- and flood-dominated. His cartoon of an idealised channel system is presented in Fig. 5.4(b). It shows

a single meandering ebb-dominated channel separated by shoals from the flood-dominated side channels. The pattern resembles the one in the model estuary presented in Fig. 5.2.

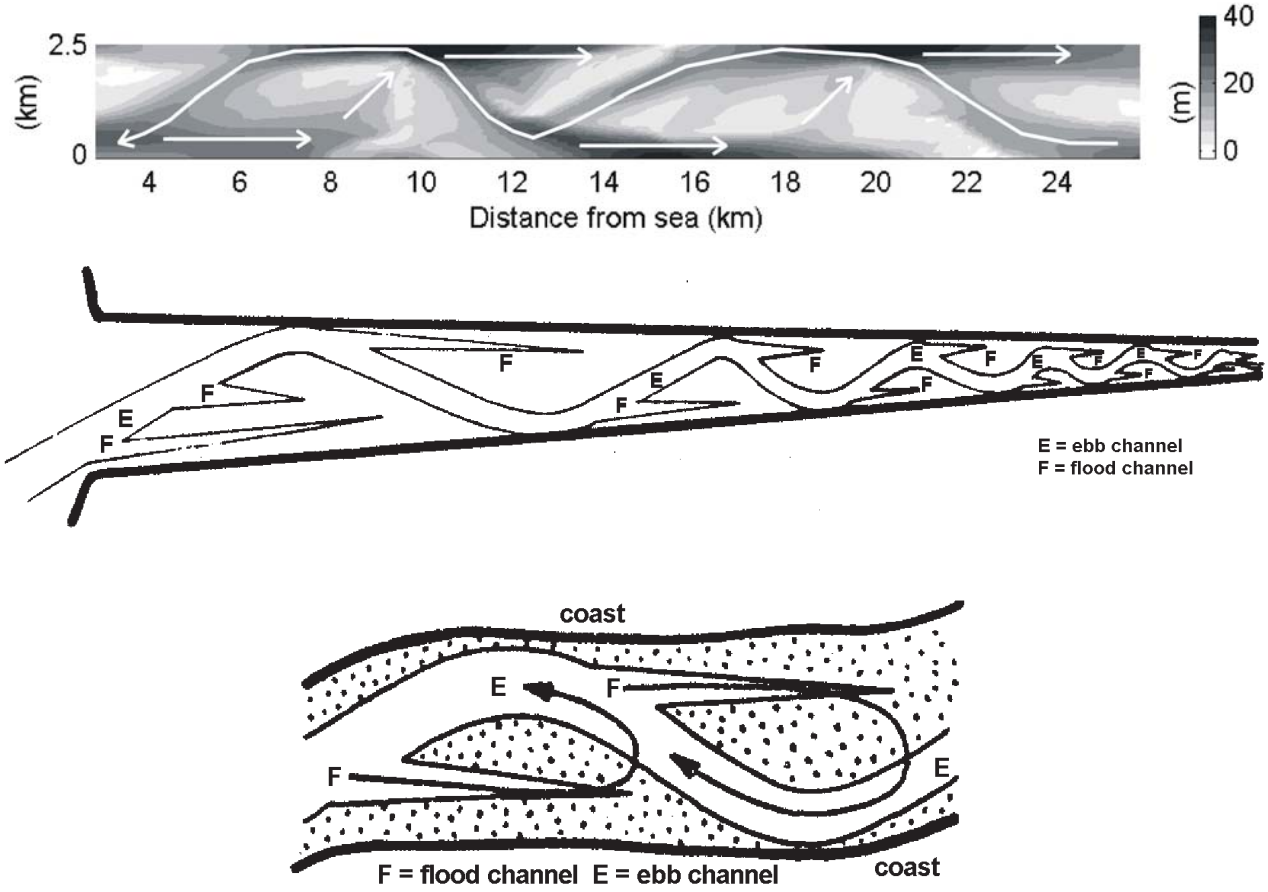

Figure 5.4: (a) Seaward part of the model simulation. The trajectories indicate the direction of the residual velocity. (b) Sketch of an idealised ebb(E)- and flood(V)- channel system by Van Veen (1950). (c) Sketch of "circulating sand currents" by Van Veen (1950).

The similarity is confirmed by the tidally-averaged flow pattern of the model simulation. Fig. 5.4(a) shows a continuous ebb-dominated meandering flow, with flood dominance found in interrupted channels aligned with the lateral boundaries. This pattern results in a water and sediment circulation pattern like the one observed by Van Veen (see Fig. 5.4(c)). Van Veen attributes the existence of a bar at the end of each flood channel to three-dimensional sediment transport mechanisms. Since similar features are found in the depth-averaged model, even when using a sediment transport formula, this explanation does not hold.

In the landward part of the model estuary, the pattern is different: the flood-dominated channels do not end in a shoal and they are not aligned with the lateral boundaries. In fact, they meander in a similar way as the ebb-dominated channels (last panel Fig. 5.3). This yields a pattern that can be characterised as a sequence of braided ebb- and flood-meanders with shoals in between.

Such a pattern can also be observed in the Western Scheldt estuary. A section of this estuary, 40 km landward of the mouth, is presented in Fig. 5.5(a). The direction of the residual current in the channels is indicated in the figure. The length of the two cells is 25 km, which is twice the wavelength of the pattern in the simulation. This is probably due to the fact that the aspect ratio of the Western Scheldt estuary is about twice the one in the model. This is substantiated by a simulation of a 5 km wide basin, which predicted channel wavelengths of about 20 km in the seaward part of the estuary.

Field observations of this feature on a smaller scale are reported by Ahnert (1960), for the estuaries around the Chesapeake Bay area. He described the pattern in the Patuxent River estuary as a succession of oblong pools, connected by narrow channels at the bend. Underwater sandbars separate the channels in the pool. On this scale the wavelength amounts to 9 km. His cartoon of the meandering channel system is presented in Fig. 5.5(b) and shows a striking resemblance to the model results. That this braided meandering is not found at the entrance of the estuary is also observed by Ahnert: "In the estuaries around the Chesapeake Bay estuarine meanders follow a strikingly regular pattern of occurrence. They extend neither landward all the way to the head of the tide nor seaward to the mouth, but occupy a stretch in the middle part of the estuary". The explanation was found in the modification of the tidal wave. The tide enters an estuary with the characteristic properties of a progressive wave, when the maximum flood current occurs at high tide and the maximum ebb current at low tide. As the tidal wave proceeds up the basin, the maximum water level lags behind the maximum current. This time difference increases until the maximum ebb and flood current occur at approximately mean water level. Thus the maximum strength of both currents is comparable and therefore causes comparable lateral erosion. At the entrance of the model estuary the time lag between extreme tide and maximum currents is already around two hours. This time difference increases further landwards, causing a decrease of water level difference at maximum currents. However, slack water at extreme tides, as observed by Ahnert, is not reached. These observations can best be illustrated by the hydrodynamics on the initial profile. In Fig. 5.6 the water level and currents during one tidal period at the entrance and halfway up the basin are presented analogous to a figure in Ahnert (1960). The grey columns mark the time period during which the current velocity is more than 90% of the maximum. The horizontal lines indicate the maximum water level during this high ebb current and the minimum water level during high flood currents. Halfway up the estuary (right panel), where the previously described features form, a range of water levels exist at which both ebb and flood currents flow with more than 90% of maximum velocity, indicated by the grey horizontal bar. At the mouth (left panel), this overlap in water levels is not present. Despite the changes in the hydrodynamics due to the formation of channels and shoals and the development of the longitudinal profile, the overlap in water levels present at high ebb and flood currents persist halfway the estuary but do not occur at the mouth.

In addition to this hydrodynamic cause for differences in patterns, the width-to-depth ratio of the estuary is also found to be important. This is obvious for the initially formed undulations.

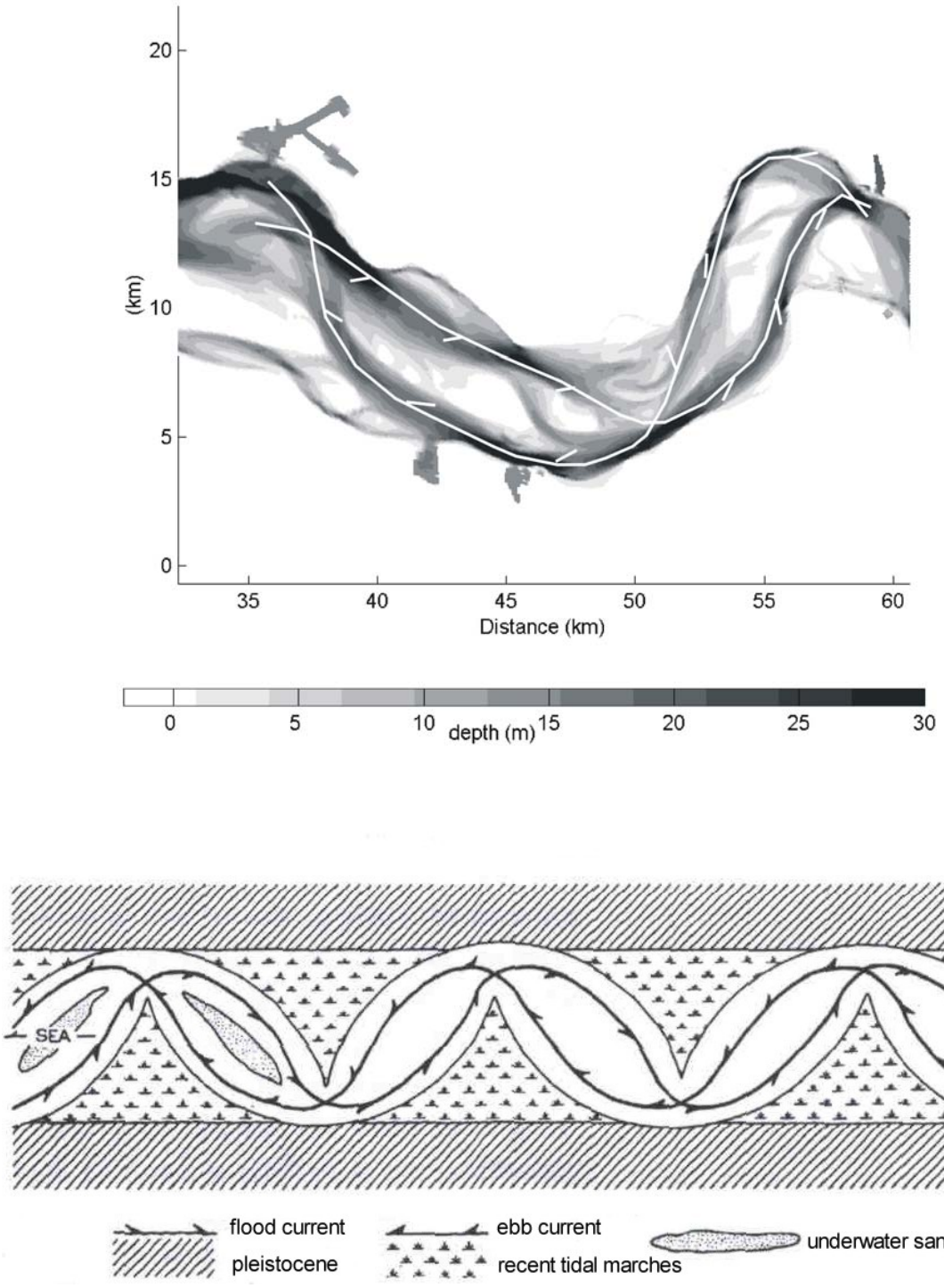

Figure 5.5: (a) Section of the Western Scheldt estuary, the Netherlands, 1996. The trajectories indicate the direction of the residual velocity. (b) Sketch of meandering channel system by Ahnert (1960).

The deepest part of the estuary exhibits an alternating pattern of erosion and deposition. Further landwards, the depth decreases and so does the wavelength of the undulations. Sev-

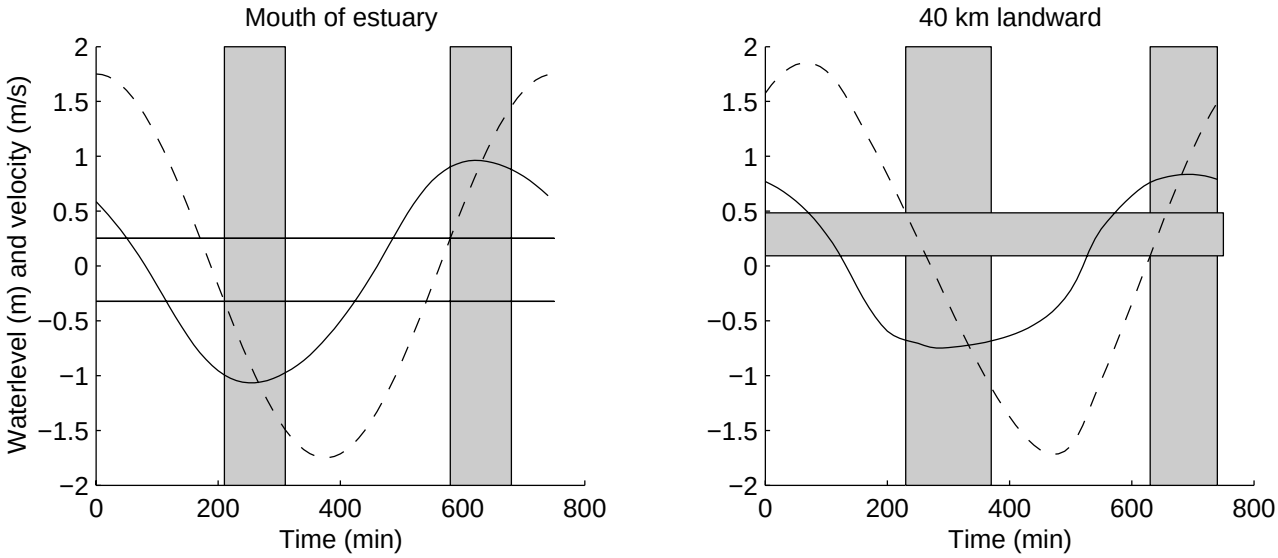

Figure 5.6: Water level (dashed) and velocity (line) at the mouth of the estuary (left panel) and halfway up the estuary (right panel). Ebb velocities have a negative sign, flood velocities are positive (see text for explanation).

eral zero-crossings occur over the width of the basin (Fig. 5.3, panel 4). Although the initial undulations gradually merge into larger-scale patterns, the wavelength increase from land to sea remains. Field observations in various estuaries imply that as the width-to-depth ratio increases, more multiple rows or braided bars are produced (Dalrymple and Rhodes, 1995). For a width-to-depth ratio less than approximately 100, alternate bars are produced. This can be associated with a meandering flow in a straight channel, as in their context, bars are part of the channel. The length of the alternate bar pattern is found to be six times the channel width, i.e. 15 km for a 2.5 km wide estuary, in good agreement with our model result. The width-to-depth ratio at the mouth of the estuary, however, is 160, using the cross-sectional mean depth in the ratio. This is considerably larger than 100. The latter value is only found if the channel depth is used in the ratio, instead of the cross-sectional mean depth. An example of the braided bars forming in shallow areas is presented in Fig. 5.7, which result from the simulation that uses the advection-diffusion equation to predict suspended sediment transport. In this area the initial water depth with respect to MSL varies from 4 to 1.5 m, which corresponds with a width-to-depth ratio of 625 to 1666. The height difference from channel bottom to bar crest in this pattern is smaller than in the deeper parts of the estuary, in accordance with the observations of Dalrymple and Rhodes (1995).

5.6 Discussion

In the previous sections is shown that the numerical model can reproduce the formation of channels and shoals in an idealised estuary. The mechanism responsible for the formation is

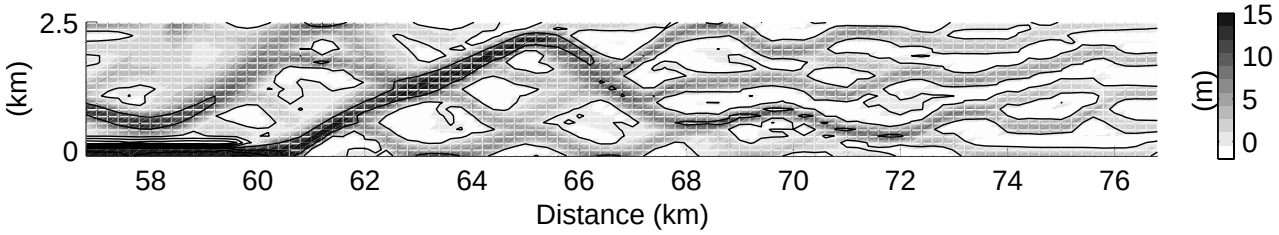

Figure 5.7: Multiple channel system for large width-to-depth ratios.

probably a positive feedback mechanism between current and bathymetry. The initial perturbations of the bed induce small perturbations in the velocity field that impact sediment transport and ultimately influence bottom changes. Thus the final morphology at the end of this chain of processes is the result of the bathymetry itself, forming a feedback mechanism. The initial perturbation appears to be necessary to trigger the pattern formation. A model simulation of the previously described basin that omits the initial disturbances, does not form a 2–D pattern but only adjusts of the longitudinal profile. A random initial perturbation develops into a regular pattern that can be described by a characteristic wave length. Apparently the feedback mechanism is positive for this wave length. Why exactly this wave length emerges, while a random perturbation contains many other wavelengths, remains to be investigated. It is related to depth and current velocity, but because these parameters are also mutually related, it is difficult to specify the exact/quantitative relation.

Models based on stability analyses give more insight into the physics underlying the morphodynamic processes. This type of models are used by Seminara and Tubino (1998, 2001) and Schuttelaars and De Swart (1999, 2000) to demonstrate that channels and shoals can develop due to a positive feedback between tidal currents, sediment transport and bedforms. The formulations and assumptions in these analytical models differ from each other and from our process-based model. Therefore their conclusions do not straightforwardly apply for these model results. Schramkowski et al. (2002) extended the model of Schuttelaars & de Swart (1999, 2000) to study bottom patterns in estuaries similar to these considered by our model. The stability analysis shows that the bottom patterns are formed by the combined effect of bottom friction and advection. The residual flow induced by tide-topography interactions causes net sediment fluxes towards shoals and away from deep channels. Bed slope effects dampen the small scale features and the length scale of the resulting fastest-growing bars is of the order of the tidal excursion length (~ 7 km). This is in accordance with our model, where the wavelengths of the initially growing undulations vary between 3 km in the shallow areas to 10 km in deeper water.

For a thorough comparison of the results, the model assumptions have to agree more closely. One fundamental problem is that stability analyses start from a so-called basic state, which is a steady equilibrium solution of the mathematical model. This may be relaxed to a solution that varies on a much slower time scale than the undulations to be investigated. The numerical

model, however, starts from an arbitrary initial topography, and allows the mean profile and the channel–shoal pattern to evolve concurrently. In analytical models, the basic state can be computed a priori, but this is not possible in the numerical model. Using the analytical basic state as an initial profile in the numerical simulation requires close agreement of the model assumptions, otherwise the numerical model starts adjusting the profile while the undular patterns emerge. At present our model only concludes that local changes to bed level due to the initial pattern formation are up to an order of magnitude larger than the changes in the width-averaged longitudinal profile. A preliminary comparison of the evolution of this longitudinal profile with the equilibrium profiles of Schuttelaars and de Swart (2000) shows some agreement, especially the deepening near the entrance of the basin and the steepening of the landward slope. A full mutual comparison of the numerical and the analytical models is done by (Hibma et al., 2003b), described in Chapter 3. This requires an adapted version of the present process-based modelling system, where the model formulations resemble the descriptions in the analytical model.

The subsequent development of the undulations into larger scale patterns falls out of the scope of stability analyses, because the processes are highly non-linear. During this process the channels deepen, the shoals grow and the wave lengths increase. The current velocities in the developing channels increase, which can explain the increase of length scale through the associated increased inertia. At the end of the simulation the inter tidal shoals have reached an average height of 1.0 m below the local mean water level. While locally the sills at the junction of channels remain morphologically active, the overall large scale pattern is more or less stable. The stability depends both on an equilibrium between morphology and currents, and on the presence of non-erodible lateral boundaries. These prevent further lateral movement and associated dynamic behaviour in the channels. The boundaries will therefore also influence the length scale of the pattern in the developed stage. During the initial formation the length scales of the bed patterns are smaller than the width of the basin and the boundaries do not significantly influence on the length scales or processes. The conclusions are substantiated by sensitivity simulations for variable basin widths. The model formulation also neglected wind waves. During the simulation the shoals attain shallower depths, which would result in increased wave influence. In the type of estuary studied for this paper – a long inland basin – waves are typically moderate. In the long run, they probably influence the average height of shoals, as this decreases during storms and increases during calm weather periods (De Vriend et al., 1989). The influence of this phenomenon on overall pattern formation is expected to be minor however, and therefore neglected in the present analysis.

Despite inherent limitations, the simplified geometry and the basic parameter setting contribute to the transparency and generalisation of the obtained results. Most model parameters only influence the length scale of the patterns or the time scale of the formation, but the underlying processes remain the same. However, the neglect of waves and large river runoff limit the validity of the model to elongated inland estuaries, that are tidally dominated and well-mixed.

5.7 Conclusion

The channel–shoal patterns emerging from the numerical simulations agree with patterns that are known from nature. The initially formed undulations seem to correspond at least qualitatively with the results of the linear stability analyses of Schramkowski et al. (2002), although a full mutual comparison was not feasible, due to the differences in model assumptions and formulations.

The relatively simple initial pattern of erosion and deposition, once it has reached a finite amplitude and therefore has become subject to non-linear interaction processes, increases in spatial scale and forms specific, quasi-regular patterns of channels and shoals. The global pattern is stable after approximately a century. These realistic channel–shoal patterns are produced by a 2–D depth-averaged numerical model. Within the parameter ranges considered, the results seem to be insensitive to the specific sediment transport formulation applied. In a later phase, the interaction with mudflats and marshes should be included, introducing cohesive sediment and vegetation, in order to simulate the large-scale evolution of natural systems.

Appreciating the need for further validation and analysis, it can be concluded that this model provides a tool, complementary to fieldwork, theoretical behaviour analyses and laboratory experiments, for the analysis of the large-scale morphological behaviour of estuaries and tide-dominated coastal lagoons.